Hindawi
International Journal of Antennas and Propagation
Volume 2024, Article ID 5522356, 13 pages
https://doi.org/10.1155/2024/5522356

Research Article

A Compact Isolated CR Antenna System for Application in C-Band

Rajeev K. Parida,[1] **Abdulkarem H. M. Almawgani**,[2] **Arjuna Muduli**,[3] **Dhruba C. Panda**,[1] **Adam R. H. Alhawari**,[2] **Amrindra Pal**,[4,5] **M. M. Abdullah**,[6,7] **and Hasan B. Albargi**[6,7]

[1]*Electronic Science and Technology, Berhampur University, Berhampur 760007, India*
[2]*Department of Electrical Engineering, College of Engineering, Najran University, Najran 11001, Saudi Arabia*
[3]*School of Electrical and Communication Sciences, JSPM University, Nagar Road, Wagholi, Pune 412207, India*
[4]*National Research Foundation Nepal, Bijulibazar, Kathmandu 44600, Nepal*
[5]*Department of ECE, University Centre for Research and Development, Chandigarh University, Gharuan, Mohali 140413, India*
[6]*Department of Physics, College of Science and Arts, Najran University, Najran 11001, Saudi Arabia*
[7]*Advanced Materials and Nano-Research Centre (AMNRC), Najran University, Najran 11001, Saudi Arabia*

Correspondence should be addressed to Amrindra Pal; amrindra.ieee@gmail.com

Received 6 July 2023; Revised 10 February 2024; Accepted 20 February 2024; Published 15 April 2024

Academic Editor: Arpan Desai

In this work, a dual-port antenna system is simulated and fabricated for cognitive radio (CR) application. The proposed system comprises a tapered-fed monopole ultra-wideband (UWB) sensing antenna and a dual-narrowband (NB) communicating antenna. For miniaturization, the UWB sensing antenna is placed on the front side of the communicating antenna. The sensing operation takes place over 2.1–12 GHz. The E-shaped dual-band antenna operates at 3.9 GHz and 6.04 GHz. The envelope correlation coefficient (ECC) and isolation are measured to be lower than 0.12 and greater than 18 dB, respectively, within the range of acceptable values for both parameters. The antenna prototype was fabricated and tested experimentally to confirm the simulation's findings. The outcomes of both the simulation and the testing revealed a definite consistency. This work gives a miniaturized model and good isolation, which is appropriate for C-band applications.

1. Introduction

As per the FCC (Federal Communication Commission), about 70% of allocated electromagnetic spectrums still need to be fully utilized. Cognitive radio (CR) technology appeared as a viable option for optimal utilization of the electromagnetic spectrum [1, 2]. After interacting with the radio environment, the CR automatically modifies the radio transmitter parameters. Effective spectrum management is only conceivable for CR with its antenna system. The cognitive radio antenna module consists of an ultra-wideband (UWB) spectrum sensing antenna and a narrowband (NB) communication antenna [3–6]. However, designing an efficient antenna module for deployment inside CR satisfying key requirements such as good isolation, reduced physical dimensions, and multiband characteristics is challenging [7, 8].

In the last decade, multiport-based antenna systems have been adopted for designing the CR antenna system. Multiport-based models can be used for continuous and instantaneous spectrum sensing and communication within the accessible frequency spectrum. The consideration of isolation is a crucial aspect in the design of a multiport system [9, 10]. Several methodologies have been introduced and published in the literature [11–16]. The techniques that are adopted for obtaining good isolation are (1) antenna placement and orientation [12], (2) defected ground structures (DGSs) [13], (3) slots/slits-etching [14], (4) protruding ground stub structures [15], and (5) parasitic elements/structures [16]. In addition to this, other popular techniques are discussed in [17–25], as follows: (1)

metamaterials (MTMs)-split-ring-resonator (SRR) [18]; complementary-split-ring-resonator (CSRR) [19](2) electromagnetic band gap (EBG) structure [20], (3) decoupling and matching network [21], neutralization line [22], (4) cloaking structures [23], (5) shorting vias and pins [24], and (6) inherent or no isolation techniques [25]. To minimize the dimension of the CR antenna, the radiating patch of one antenna acts as the ground plane of the other [26]. Various reconfiguration mechanisms using a stepper motor, PIN diode, LASER, etc. are incorporated into the communication antenna for communicating in the entire band recognized by the sensing antenna. These configurations suffer from bulkiness, slow tuning, negative effect of biasing lines, power consumption, and nonlinearity effects [27–29]. Nowadays, combining patches in a small space without interrupting surface current distribution and ensuring sufficient isolation between the antennas are factors to consider. In addition, in the current scenario [30], there is a great demand for compact and portable antenna systems for specific applications in the C-band.

To address the above challenges, a two-port antenna system (UWB sensing + multiband (E-shaped) communication) is designed for cognitive radio applications to increase spectrum utilization efficiency, which is the primary goal of our research. This paper proposes a new CR antenna consisting of a tapered-fed UWB monopole as the sensing antenna and a dual-band E-shaped patch as the communicating antenna. For the miniaturization of the module, we put the UWB sensing antenna on the top side of the dual-band antenna. In addition, good isolation is obtained between the antennas because of the feeding diversity of both antennas; one is a microstrip line, and the other is co-axial feeding. Performance optimization of the whole structure is done using CST microwave studio.

2. Antenna Structure Design and Configuration

Figure 1 depicts aerial views of the CR antenna. It has a FR-4 substrate ($\varepsilon_r = 4.4$, $\sigma = 0.02$). The overall size is 40 mm (Ws) × 50 mm (Ls), and thickness of the substrate is $h = 1.6$ mm. For the dual-band antenna, the radiator portion of the UWB sensing antenna acts as a ground plane. The E-shaped patch (Port-2) is placed on the backside of the substrate. Table 1 shows the proposed model geometry. The methodology is algorithmically represented in Figure 2, which indicates a transparent explanation of the design process.

2.1. UWB (Sensing) Antenna. A triangularly tapered feeding mechanism is used for designing the UWB antenna (Figure 1(a): Front side). For good impedance matching, the ground is a partial ground plane. The lower band-edge frequency f_L of the proposed UWB monopole is defined using the following equation (1) [31]:

$$f_L = \frac{C}{\lambda} = \frac{7.2}{\{(L + r + g) \times k\}}\ \text{GHz}, \tag{1}$$

where L, r, and g are the length, radius, and gap between the radiating patch and ground plane, respectively, and f_L is the lower cut-edge frequency for the proposed antenna. For $\varepsilon_r = 4.4$, the optimum value of $k = 1.2$ is chosen empirically. The optimal value of feed line length L_f is found using Riccati equation [32] as shown in the following equation:

$$\Gamma(\theta) = \frac{1}{2} e^{-j\beta L_f} \left(\ln \frac{Z_{L_f}}{Z_0} \right) \left[\frac{\sin\left(\beta L_f/2\right)}{\left(\beta L_f/2\right)} \right]^2, \tag{2}$$

where Z_{L_f}, β, Z_0 and $\Gamma(\theta)$, are the load impendence, phase constant, characteristic impedance, and reflection coefficient, respectively. Iterative optimization is used to determine the feed line widths W_{f1} and W_{f2}. This factor (i.e., the width of feed line) is independent of the resonance frequency.

2.2. Narrow-band Communicating Antenna. Figure 1(b) shows the dual-band E-shaped communicating antenna. The E-shaped antenna has two identical notches made symmetrically on both sides of the feed location. Its dual-band property depends on the symmetrical notch, which increases the length of the current path and consequently changes the values of C and L [33]. Due to the change in L and C values, another frequency band is created in addition to the fundamental frequency band. The dimensions of the E-shaped antenna are calculated using [34, 35].

3. Results and Discussion

Figure 3 shows the CR antenna module fabricated using an MITS PCB prototyping machine. The return loss performances and the radiation characteristics of the CR antenna were measured using a VNA and observed in the anechoic chamber, respectively. In a triangularly tapered-fed antenna, instead of using a full ground plane, a partial ground plane yields better impedance matching (Figure 4). Figures 5 and 6 show the parametric study (by varying "L_g" and feed-gap "g") of the UWB antenna. These two factors significantly affect impedance matching and bandwidth [31]. Figures 7 and 8 show the simulated and measured return loss performances. The sensing UWB antenna at Port-1 gives a wider bandwidth from 2.1 to 12 GHz (Figure 7). The communicating (NB) E-shaped antenna at Port-2 operates at two different frequencies. The 1st resonating mode is at 3.9 GHz, and the 2nd mode is at 6.04 GHz (Figure 8). The discrepancies between simulated and measured plots can be seen due to fabrication errors, surrounding cable losses, and spurious radiation from the coaxial probe mounted on the monopole during measurement [28]. Figure 9 shows the simulated VSWR plot (<2 in the operating band) of the CR antenna.

3.1. Group Delay and Phase Response. The time domain performance is assessed using group delays (GDs), the magnitude of S_{21}, and phase response. CST microwave studio is used to perform the time domain analysis. It is based on the finite integration approach (FIT). The study analyzes the time domain performance on two identical ultra-wideband (UWB) antennas. These antennas are positioned 100 mm from each other in the far-field region [36]. The investigation is undertaken in two orientations: face-to-face (FTF) and side-by-side (SBS). The calculation of group delay (τ) quantifies the temporal discrepancy (time delay) incurred by a signal throughout its propagation from

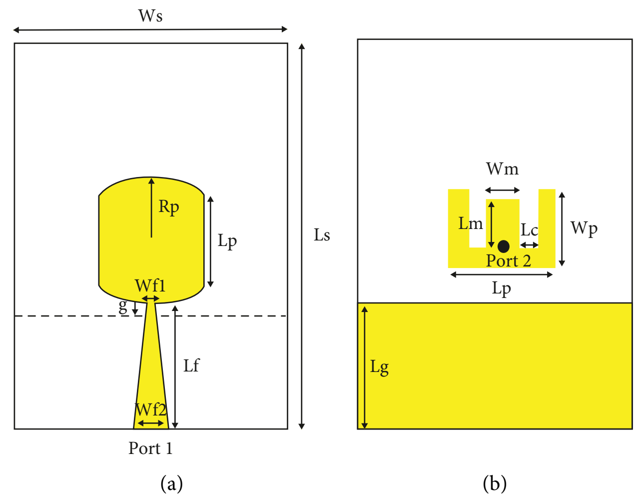

Figure 1: Proposed antenna (a) top view and (b) rear view.

Table 1: Design parameters of the proposed CR antenna.

Parameters	Size (mm)
W_s (sub. width)	40
L_s (sub. length)	50
R_p	12
L_p	14
L_f	16.5
W_{f1}	1.5
W_{f2}	3
L_g (ground length)	16
L_c	1
g	0.5
W_p	11.5
L_p	15
W_m	8
L_m	8.5

the point of transmission to the point of reception. The calculation for the group delay is as follows: $\tau = -(d\theta(\omega)/d\omega)$

where θ is the signal phase (in rad) and ω is the frequency (in rad/s). In order to plot GDs in CST, we must go through the following 6 crucial procedures in sequential order: (1) postprocessing (template post-processing), (2) time signals, (3) group delay, (5) determine the receiver and transmitter ports as well as relevant modes, and (6) evaluate. Figure 10 shows that the group delay response appears consistent and flat across the frequency range (an acceptable value is less than 3 ns [37]). It implies that the proposed antenna is non-dispersive. Similarly, to plot the magnitude and phase response (S_{21}), we follow the steps: (1) 1D results, (2) S-parameters (S_{21}: magnitude (dB)), and (3) S-parameters (S_{21}: phase (degrees)) in sequential order. Figures 11 and 12 show that, up to 10.6 GHz, the magnitude remains almost constant (better than −20 dB), and the phase response is linear (in both the FTF and SBS configurations). Nonlinearities in phase response and magnitude response become detectable at frequencies over 10.6 GHz [38]. This is because the substrate and antenna geometry can indeed influence an antenna system's group delay and phase response.

3.2. Gain and Radiation Patterns. The 2D radiation patterns of both the sensing and communicating antenna are illustrated in Figures 13 and 14. In both planes, the UWB antenna exhibits an omnidirectional pattern in the H-plane and a directive pattern in the E-plane (Figure 13). The partial ground plane deteriorates the polarization purity at higher frequencies. Also, some discrepancies were observed mainly due to fabrication errors and surrounding cable losses during antenna measurement. It clearly shows that the simulated results of both UWB/NB antennas agree well with the measured values. The simulated gains are 2.27 dBi, 4.7 dBi, and 6.16 dBi at 3.85 GHz, 5.98 GHz, and 10.02 GHz for a sensing antenna, respectively. The simulated and measured gain of the UWB antenna is shown in Figure 15. Similarly, for the communicating antenna, they are 1.9 dBi, 4.81 dBi at 3.9 GHz and 6.04 GHz, respectively. The radiation efficiency of the CR antenna is shown in Figure 16. Due to the absence of higher-order modes, the radiation efficiency is maximum at the lowest matching frequency and deteriorates marginally to 70% as higher-order modes appear with increasing frequencies. Therefore, the efficiency gradually degraded at higher frequencies due to increased losses. The copper and substrate losses are frequency-dependent and increase with frequency [39–41]. Figure 17 depicts the E-field and H-field radiation pattern measurement setup.

3.3. Isolation Mechanism and Surface Current Distribution (SCD). Figure 18(a) depicts the SCD of the UWB sensing antenna without the communicating antenna at 3.85 GHz, 5.98 GHz, and 10.02 GHz. The current distribution plots show that the maximum current lies at the edge of the radiating patch and the edge of the partial ground plane. Therefore, the center part of the radiating patch is an appropriate position to integrate the NB antenna to produce better isolation due to minimal surface current

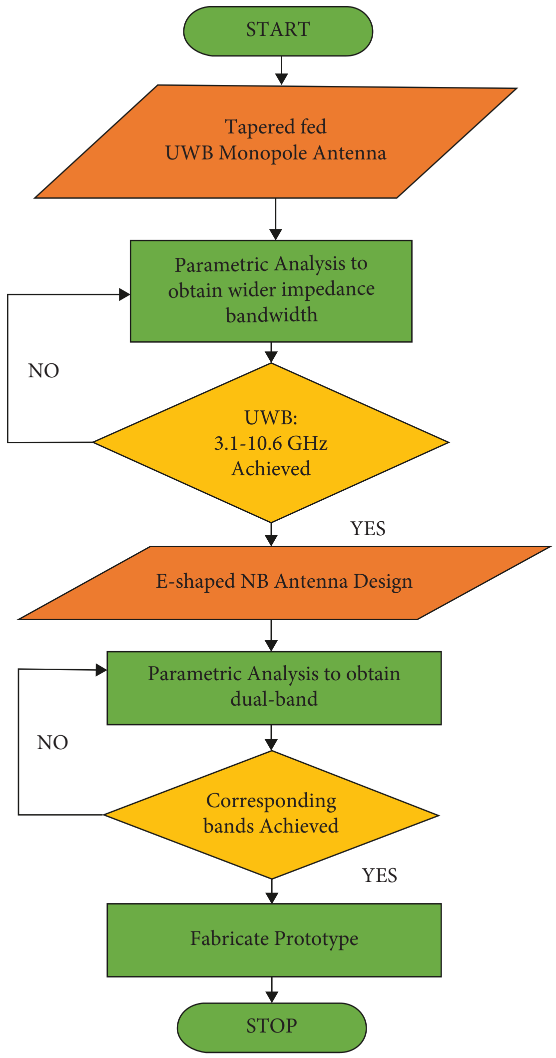

Figure 2: Flowchart of antenna design methodology.

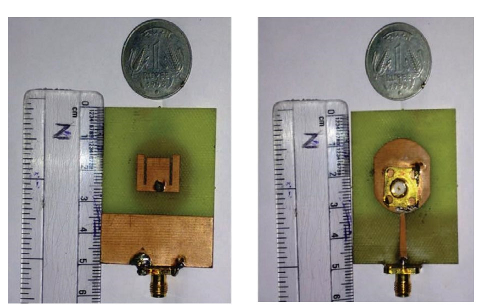

(a) (b)

Figure 3: Fabricated prototype (a) bottom view and (b) top view.

density. Figure 18(b) shows the SCD of antenna-1 (sensing UWB antenna: Port-1 excited) while the E-shaped NB antenna (Port-2) is terminated. In such cases, minimum current flows in the NB antenna while maximum current flows at the edge of the UWB antenna when Port-1 is excited. Similarly, Figure 18(c) indicates the SCD of antenna-2 (E-shaped NB antenna: Port-2 excited) while the sensing antenna (Port-1) is terminated [42]. In this case, the maximum current flows in the NB antenna compared to those in the UWB antenna when Port-2 is excited. This is observed both at 3.9 GHz and 6.04 GHz, as the UWB radiator acts as a ground plane for NB antenna. A minor surface current magnitude seems to exist in the UWB structure. This minor surface current magnitude does not affect the radiation behavior of the NB antenna, which was validated by observing the ECC (below 0.5).

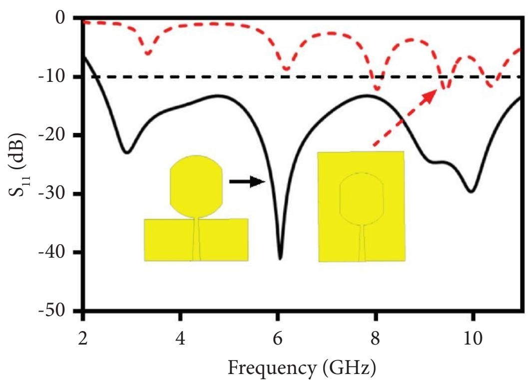

Figure 4: UWB antenna using different ground structures.

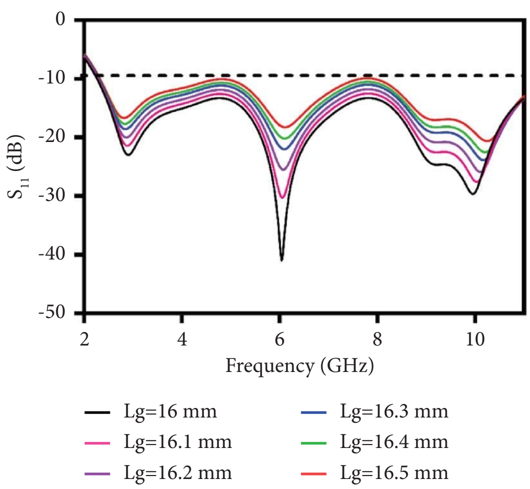

Figure 5: Parametric study of UWB antenna by varying ground length (L_g).

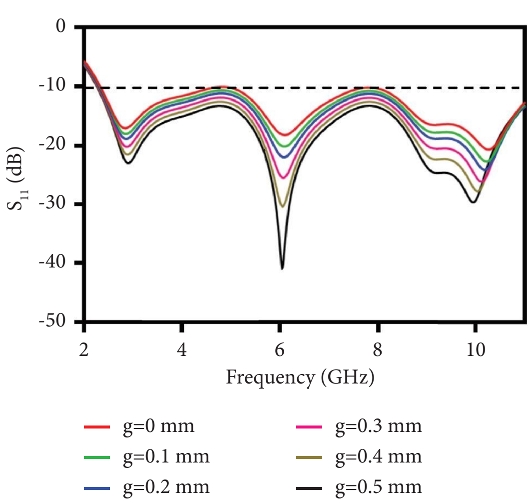

Figure 6: Parametric study of UWB antenna by varying feed-gap (g).

The measured and simulated isolation curves are depicted in Figure 19. It reveals that both antennas have minimal mutual coupling, below 18 dB, throughout the

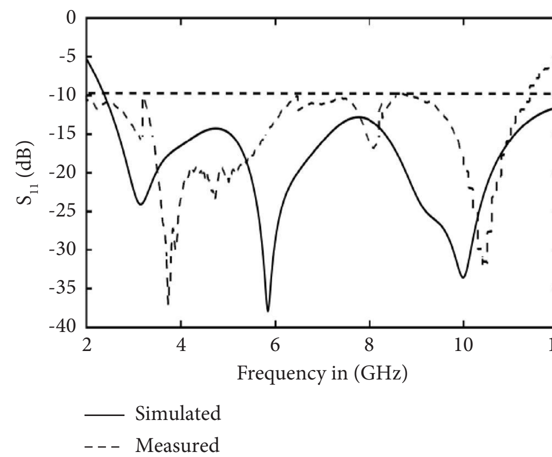

Figure 7: Measured and simulated S_{11} of the sensing antenna.

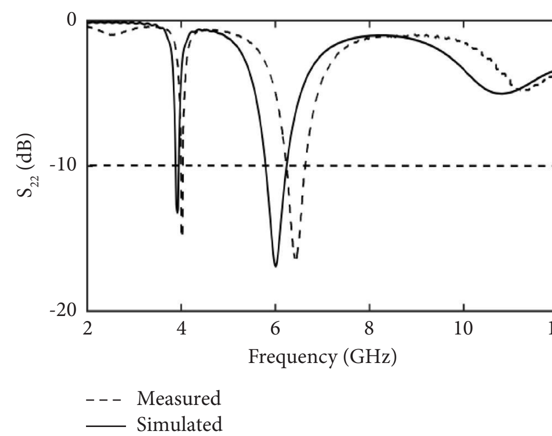

Figure 8: Measured and simulated S_{22} of communicating antenna.

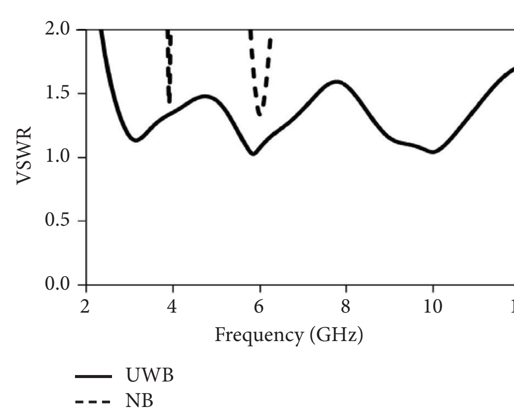

Figure 9: Frequency vs. simulated VSWR of the CR antenna.

desired sensing bandwidth. It is an appropriate value to reduce the crosstalk between the two antennas. In both simulated and measurement results, some discrepancy is observed. This is due to the approximation of boundary

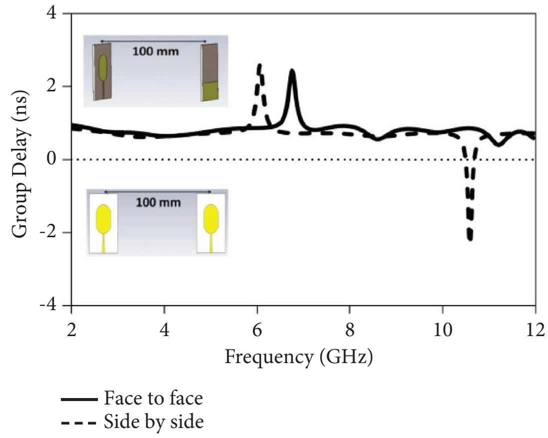

Figure 10: Simulated GDs of the UWB antenna.

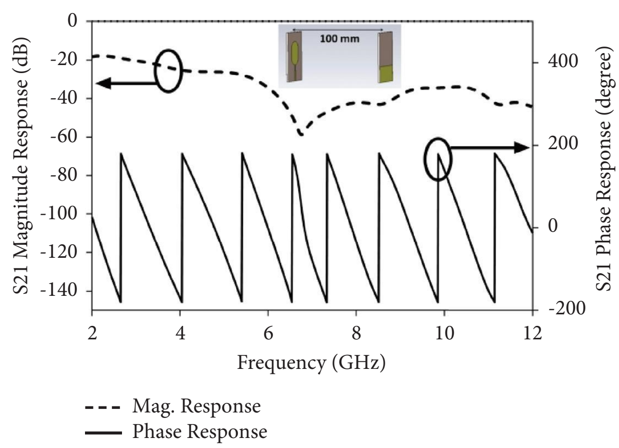

Figure 11: Simulated FTF magnitude and phase response.

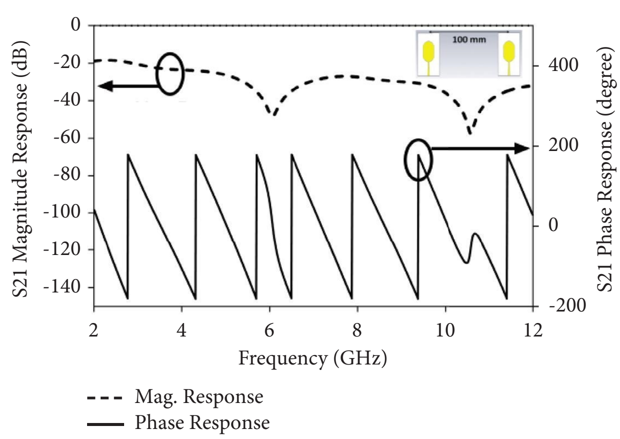

Figure 12: Simulated SBS magnitude and phase response.

conditions used in the computational package. Radio frequency (RF) cables from VNA slightly bias the measurement of miniaturized antennas [43].

3.4. ECC (Envelope Correlation Coefficient). The ECC measures the extent to which the radiation patterns are uncorrelated. It can be calculated using the following relation [10]:

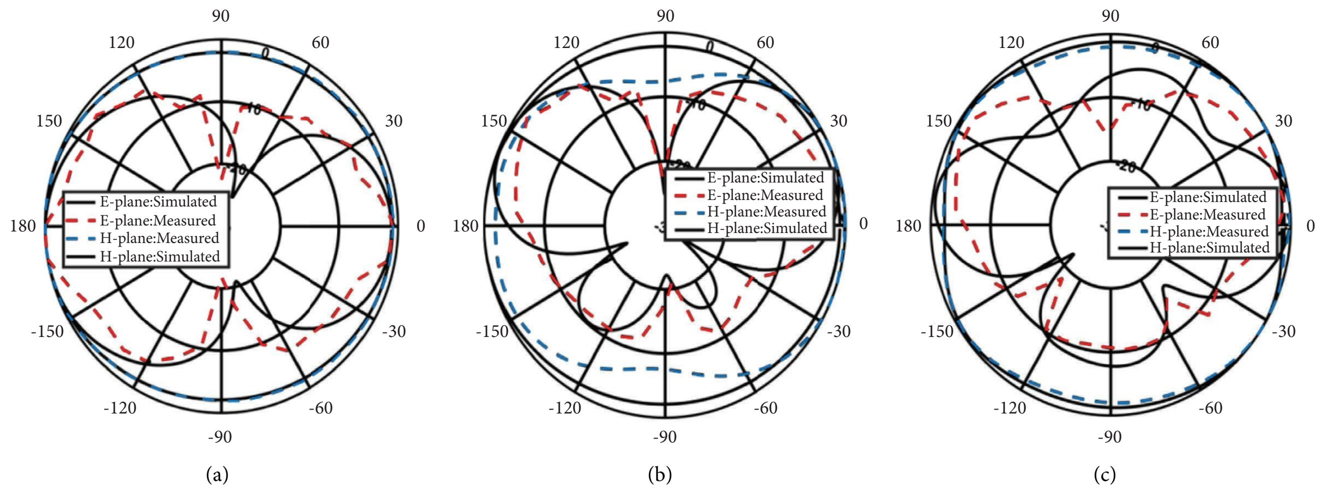

FIGURE 13: Simulated and measured radiation patterns (monopole sensing antenna) at (a) 3.85 GHz, (b) 5.98 GHz, and (c) 10.02 GHz.

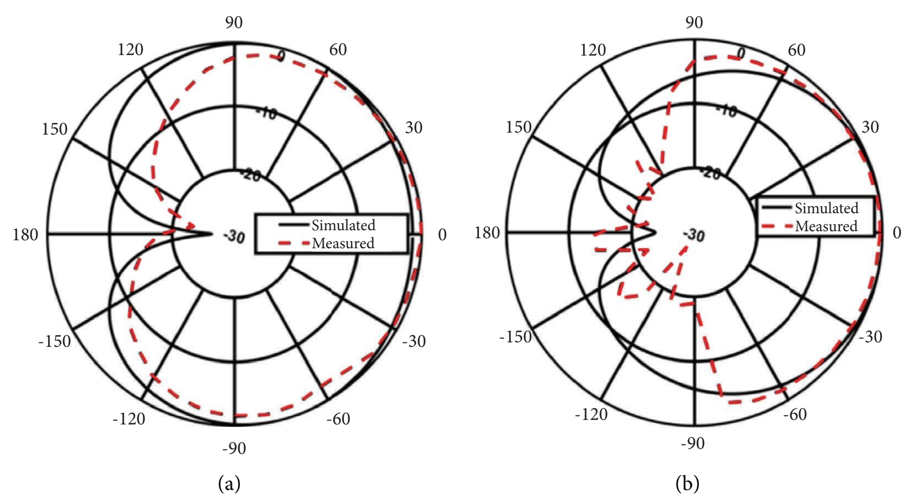

FIGURE 14: 2D-polar plot of the communicating antenna (NB) at (a) 3.9 GHz and (b) 6.04 GHz.

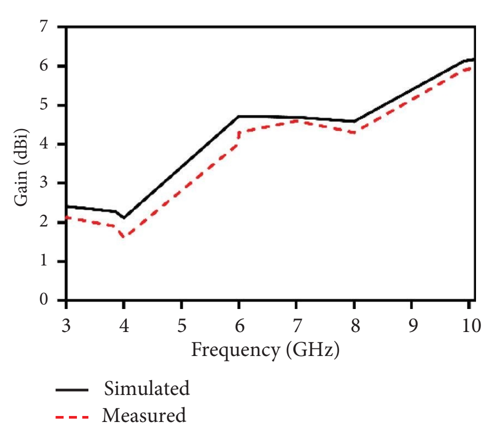

FIGURE 15: Comparison of simulated and measured gain (UWB antenna) over frequency.

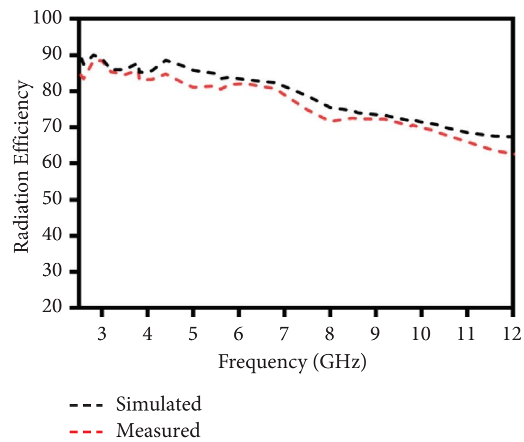

FIGURE 16: Comparison of simulated and measured radiation efficiency (UWB antenna) over frequency.

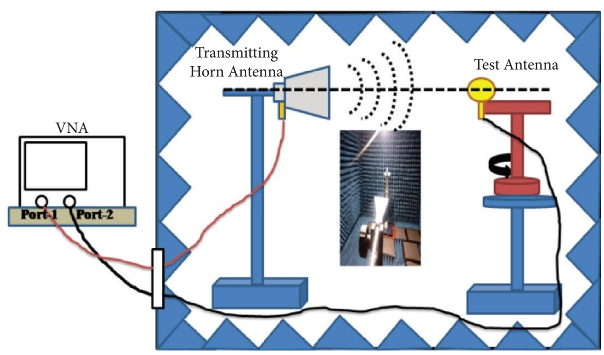

FIGURE 17: Setup inside anechoic chamber.

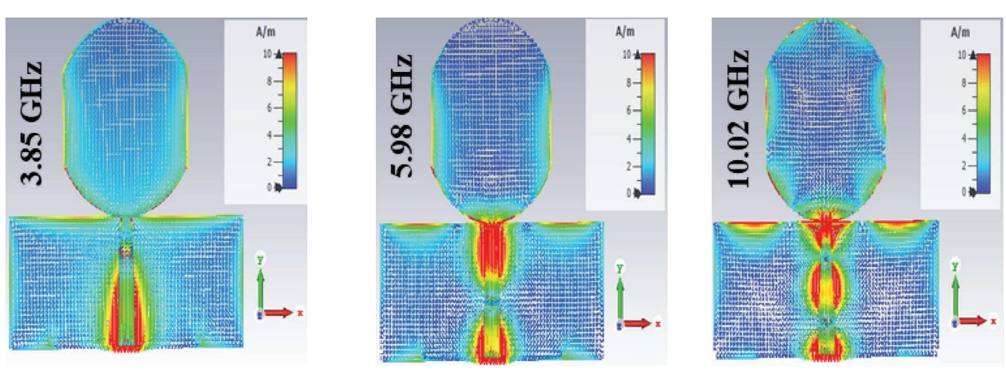

(a)

FIGURE 18: Continued.

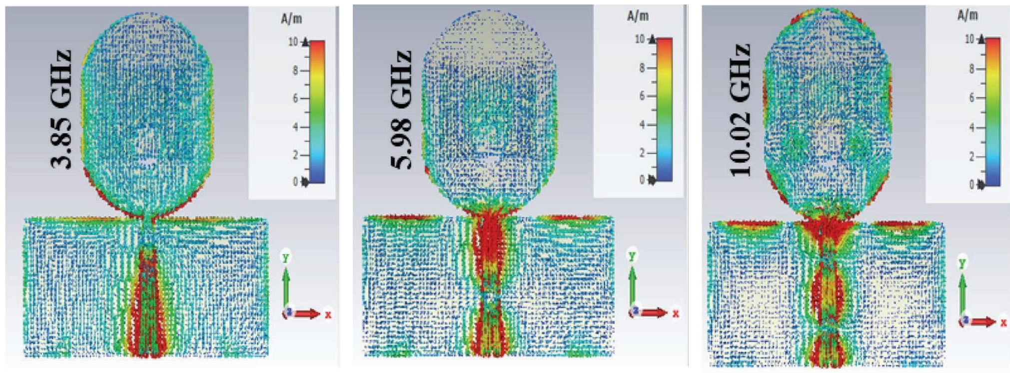

(b)

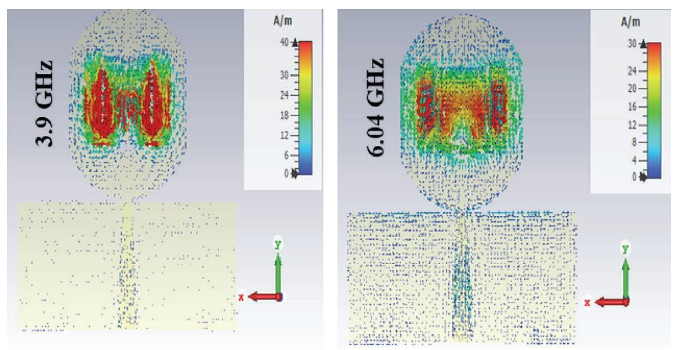

(c)

Figure 18: SCD of the proposed CR antenna.

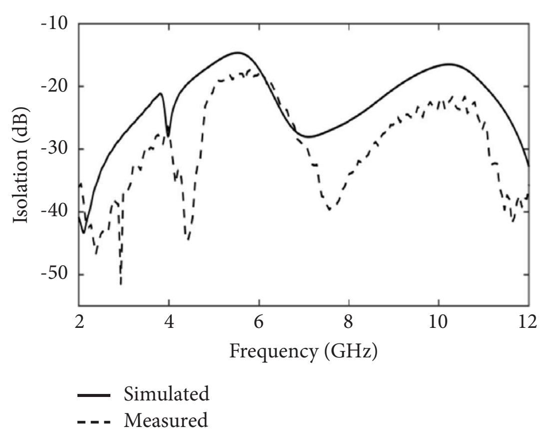

Figure 19: Comparison of simulated and measured isolations between UWB and NB antenna ports.

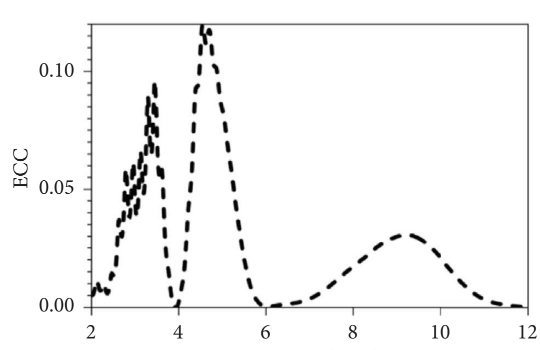

Figure 20: ECC of the proposed CR antenna.

Table 2: Detailed summaries of the recently published literature.

Published literature (year)	Impedance bandwidth for UWB antenna (GHz)	Resonating frequency for NB antenna (GHz)	Isolation between both antennas (dB)	Dimensions (mm^2)	Electrical length (λ^2)	Applications
[6] 2012	2.6–11	5.25	15	58 × 77	0.33	WLAN
[7] 2010	5.4–10.1	9.3	17	40 × 31	0.40	WiMax
[8] 2010	3.9–11	5.15	10	54 × 35	0.32	WLAN
[9] 2016	3.1–10.6	5.04, 7.6	10	75.7 × 58.35	0.46	WLAN, X-band Satellite communication
[10] 2016	2–5.5	2.8	18	80 × 65	0.22	WiMax
[44] 2017	2–12	5.65, 3.6, 5, 2.94, 4.5, 2.15 and two dual bands at 2, 5.48 and 1.7, 5	25	60 × 60	0.16	CR
[45] 2019	3.1–10.6	4.85, 5.4, 5.7, 6.7	16	50 × 30	0.16	CR
[46] 2019	3.1–10.6	2.96–5.38, 5.31–8.62, and 8.48–11.02	17.3	50 × 42	0.22	CR
[47] 2020	2–11	3.863, 4.664, 5.2, and 6.13	15	80 × 40	0.13	C-band, ISM/WLAN/military application, mid-band 5G, maritime radio navigation, X-band satellite communication, and public safety wireless communication
[48] 2021	3–11	3.25–3.7, 5.5–6.5, and 8–8.4	15	65 × 40	0.26	CR
[49] 2021	3.1–10.6	2.8–4.15, 5–6, and 7.7–11.2	17	37 × 28	0.11	5G, WLAN, LTE, and ITU
[50] 2022	2.2–11	5.54, 6.12, 7.60, 8.25, 9.64, and 10.29	18	40 × 45	0.09	CR
[51] 2023	3.1–10.6	5–11.4, 3.05–3.75, 4.9–6.1, 3.7–4.92, 8.3–11.3	16	50 × 50	0.27	CR
This article	2.1–12	3.9, 6.04	18	40 × 50	0.09	C-band communication

$$\rho = \frac{\left|S_{11}^{*}S_{12} + S_{21}^{*}S_{22}\right|^2}{\left(1 - \left|S_{11}\right|^2 - \left|S_{21}\right|^2\right)\left(1 - \left|S_{22}\right|^2 - \left|S_{12}\right|^2\right)}, \quad (3)$$

whenρ is greater than or equal to 0.5, it means a significant degradation of the radiation pattern. From Figure 20 it can be observed that the ECC exhibits very small values between 0 and 0.12. It reveals that the radiation patterns of the integrated structure are not correlated.

4. Comparison with Previously Reported Works

Table 2 represents the comparative study between recently reported multi-port antennas with different functionalities [46–51]. For a fair comparison, here, CR antennas with similar objectives are considered. The proposed integrated structure has a compact and low profile, providing wider impedance bandwidth and good isolation. Hence, the overall performance of the proposed design is satisfactory.

5. Conclusions

The designed two-port antenna structure for C-band applications offers a simple and efficient design that eliminates the need for complex and advanced production devices. The sensing antenna is designed to exhibit an omnidirectional radiation pattern. This characteristic is desirable for applications where the antenna needs to communicate with multiple devices or receive signals from various angles without the need for precise pointing. Furthermore, the sensing antenna operates within a wide bandwidth ranging from 2.1 GHz to 12 GHz. This wide frequency range accommodates a broad spectrum of signals, making it versatile for various C-band communication applications. Operating at a wide bandwidth ensures compatibility with different communication standards and frequencies. In addition to the sensing antenna, the antenna structure includes an E-shaped dual-band antenna. This antenna operates at two specific frequencies: 3.9 GHz and 6.04 GHz, providing dual-band functionality. The design of the E-shaped antenna allows for efficient signal transmission and reception at these frequencies, catering to specific communication requirements. One important aspect of the antenna structure is the isolation between the two antennas. The isolation is greater than 18 dB in the desired operating band, indicating that the two antennas are well-separated and do not interfere with each other significantly. This isolation is crucial to ensuring minimal cross-talk and interference between the sensing antenna and the E-shaped dual-band antenna, enabling both antennas to perform optimally. Due to the compact nature of our E-shaped antenna, the gain is marginally small. This will be enhanced by employing various approaches for enhancing gain, which will be beneficial when a high-gain E-shaped antenna is necessary. Overall, the two-port antenna structure offers a well-designed, straightforward solution for C-band applications.

Data Availability

The data used and/or analyzed during the current study are available from the corresponding author upon reasonable request.

Conflicts of Interest

The authors declare that they have no conflicts of interest.

Authors' Contributions

Rajeev K. Parida, Abdulkarem H. M. Almawgani, Arjuna Muduli, Dhruba C. Panda, Adam R. H. Alhawari, and Amrindra Pal have directly participated in the planning, execution, and analysis of this study. All authors have read and approved the final version of the manuscript. M. M. Abdullah and Hasan B. Albargi were extensively involved in the revision of the manuscript.

Acknowledgments

The authors are thankful to the Deanship of Scientific Research at Najran University for funding this work under the Research Groups Funding program grant code (NU/RG/SERC/12/2). Moreover, the authors extend their appreciation to the DST INSPIRE Govt. of India for financially supporting R. K. Parida.

References

[1] J. Mitola and G. Q. Maguire, "Cognitive radio: making software radios more personal," *IEEE Personal Communications*, vol. 6, no. 4, pp. 13–18, 1999.

[2] P. S. Hall, P. Gardner, and A. Faraone, "Antenna requirements for software defined and cognitive radios," *Proceedings of the IEEE*, vol. 100, no. 7, pp. 2262–2270, 2012.

[3] A. Muduli and R. K. Mishra, "Modified UWB microstrip monopole antenna for cognitive radio application," in *2015 IEEE Applied Electromagnetics Conference (AEMC)*, Guwahati, India, December 2015.

[4] E. Ebrahimi, J. Kelly, and P. S. Hall, "A reconfigurable narrowband antenna integrated with wideband monopole for cognitive radio applications," in *IEEE Antennas and Propagation Society International Symposium*, pp. 1–4, North Charleston, SC, USA, June 2009.

[5] W. Wiesbeck, G. Adamiuk, and C. Sturm, "Basic properties and design principles of UWB antennas," *Proceedings of the IEEE*, vol. 97, no. 2, pp. 372–385, 2009.

[6] G. Augustin and T. A. Denidni, "An integrated ultra-wideband/narrow band antenna in uniplanar configuration for cognitive radio systems," *IEEE Transactions on Antennas and Propagation*, vol. 60, no. 11, pp. 5479–5484, 2012.

[7] J. R. Kelly, P. S. Hall, P. Gardner, and F. Ghanem, "Integrated narrow/band-notched UWB antenna," *Electronics Letters*, vol. 46, no. 12, pp. 814–816, 2010.

[8] E. Ebrahimi and P. S. Hall, "Integrated wide–narrow band antenna for multiband applications," *Microwave and Optical Technology Letters*, vol. 52, no. 2, pp. 425–430, 2010.

[9] S. Pahadsingh and S. Sahu, "A two port UWB-dual narrowband antenna for cognitive radios," *Microwave and Optical Technology Letters*, vol. 58, no. 8, pp. 1973–1978, 2016.

[10] H. Nachouane, A. Najid, A. Tribak, and F. Riouch, "Dual port antenna combining sensing and communication tasks for cognitive radio," *International Journal of Electronics and Telecommunications*, vol. 62, no. 2, pp. 121–127, 2016.

[11] A. Kumar, A. Q. Ansari, B. K. Kanaujia, J. Kishor, and L. Matekovits, "A review on different techniques of mutual coupling reduction between elements of any MIMO antenna.

Part 1: DGSs and parasitic structures," *Radio Science*, vol. 56, no. 3, 2021.
[12] M. S. Khan, A. Iftikhar, R. M. Shubair, A. D. Capobianco, B. D. Braaten, and D. E. Anagnostou, "Eight-element compact UWB-MIMO/diversity antenna with WLAN band rejection for 3G/4G/5G communications," *IEEE Open Journal of Antennas and propagation*, vol. 1, pp. 196–206, 2020.
[13] J. Zhang, S. Yan, X. Hu, and G. A. Vandenbosch, "Mutual coupling suppression for on-body multiantenna systems," *IEEE Transactions on Electromagnetic Compatibility*, vol. 62, no. 4, pp. 1045–1054, 2020.
[14] E. Fritz-Andrade, A. Perez-Miguel, R. Gomez-Villanueva, and H. Jardon-Aguilar, "Characteristic mode analysis applied to reduce the mutual coupling of a four-element patch MIMO antenna using a defected ground structure," *IET Microwaves, Antennas and Propagation*, vol. 14, no. 2, pp. 215–226, 2020.
[15] S. R. Govindarajulu, A. Jenkel, R. Hokayem, and E. A. Alwan, "Mutual coupling suppression in antenna arrays using meandered open stub filtering technique," *IEEE Open Journal of Antennas and Propagation*, vol. 1, pp. 379–386, 2020.
[16] S. R. Thummaluru, M. Ameen, and R. K. Chaudhary, "Four-port MIMO cognitive radio system for midband 5G applications," *IEEE Transactions on Antennas and Propagation*, vol. 67, no. 8, pp. 5634–5645, 2019.
[17] A. Kumar, A. Q. Ansari, B. K. Kanaujia, J. Kishor, and L. Matekovits, "A review on different techniques of mutual coupling reduction between elements of any MIMO antenna. Part 2: metamaterials and many more," *Radio Science*, vol. 56, no. 3, 2021.
[18] P. Garg and P. Jain, "Isolation improvement of MIMO antenna using a novel flower-shaped metamaterial absorber at 5.5 GHz WiMAX band," *IEEE Transactions on Circuits and Systems II: Express Briefs*, vol. 67, no. 4, pp. 675–679, 2020.
[19] R. Selvaraju, M. H. Jamaluddin, M. R. Kamarudin, J. Nasir, and M. H. Dahri, "Complementary split ring resonator for isolation enhancement in 5G communication antenna array," *Progress in Electromagnetics Research C*, vol. 83, pp. 217–228, 2018.
[20] A. H. Abdelgwad and M. Ali, "Isolation improvement of a two-port pifa for mimo using A planar EBG ground," *Microwave and Optical Technology Letters*, vol. 62, no. 2, pp. 737–742, 2020.
[21] H. Piao, Y. Jin, Y. Xu, and L. Qu, "MIMO ground-radiation antennas using A novel closed-decoupling-loop for 5G applications," *IEEE Access*, vol. 8, pp. 142714–142724, 2020.
[22] M. Li, X. Chen, A. Zhang, W. Fan, and A. A. Kishk, "Split ring resonator loaded baffles for decoupling of dual-polarized base station array," *IEEE Antennas and Wireless Propagation Letters*, vol. 19, no. 10, pp. 1828–1832, 2020.
[23] H. S. Ahmed and T. A. Elwi, "On the design of A reject band filter for antennas mutual coupling reduction," *International Journal of RF and Microwave Computer-Aided Engineering*, vol. 29, no. 8, pp. 1–11, 2019.
[24] H. Aliakbari and B. K. Lau, "Low-profile two-port MIMO terminal antenna for low LTE bands with wideband multimodal excitation," *IEEE Open Journal of Antennas and Propagation*, vol. 1, Article ID e21797, pp. 368–378, 2020.
[25] L. Sun, Y. Li, Z. Zhang, and H. Wang, "Self-decoupled MIMO antenna pair with shared radiator for 5G smartphones," *IEEE Transactions on Antennas and Propagation*, vol. 68, no. 5, pp. 3423–3432, 2020.
[26] K. R. Jha, B. Bukhari, C. Singh, G. Mishra, and S. K. Sharma, "Compact planar multistandard MIMO antenna for iot applications," *IEEE Transactions on Antennas and Propagation*, vol. 66, no. 7, pp. 3327–3336, 2018.
[27] T. Singh, K. A. Ali, H. Chaudhary, D. R. Phalswal, V. Gahlaut, and P. singh, "Design and analysis of reconfigurable microstrip antenna for cognitive radio applications," *Wireless Personal Communications*, vol. 98, no. 2, pp. 2163–2185, 2018.
[28] N. A. Kumar and A. S. Gandhi, "A compact novel three-port integrated wide and narrow band antennas system for cognitive radio applications," *International Journal of Antennas and Propagation*, vol. 2016, Article ID 2829357, 14 pages, 2016.
[29] S. D. Joseph, S. Manoj, C. Waghmare, K. Nandakumar, and A. Kothari, "UWB sensing antenna, reconfigurable transceiver and reconfigurable antenna based cognitive radio test bed," *Wireless Personal Communications*, vol. 96, no. 3, pp. 3435–3462, 2017.
[30] M. Zahid, M. M. Taqdeer, and Y. Amin, "A compact dual-band microstrip patch antenna for C-and X-and ku-band applications," *Engineering Proceedings*, vol. 46, p. 16, 2023.
[31] G. Kumar and K. P. Ray, *Broadband Microstrip Antennas*, Artech, Morristown, NJ, USA, 2002.
[32] M. Manohar, R. S. Kshetrimayum, and A. K. Gogoi, "Super wideband antenna with single band suppression," *International Journal of Microwave and Wireless Technologies*, vol. 9, no. 1, pp. 143–150, 2017.
[33] F. Yang and Y. Rahmat-Samii, "Wide-band E-shaped patch antennas for wireless communications," *IEEE Transactions on Antennas and Propagation*, vol. 49, no. 7, pp. 1094–1100, 2001.
[34] V. K. Pandey and B. R. Vishvakarma, "Analysis of an E-shaped patch antenna," *Microwave and Optical Technology Letters*, vol. 49, no. 1, pp. 4–7, 2007.
[35] B. L. Ooi and Q. Shen, "A novel E-shaped broadband microstrip patch antenna," *Microwave and Optical Technology Letters*, vol. 27, no. 5, pp. 348–352, 2000.
[36] B. Yang and S. Qu, "A compact integrated bluetooth UWB dual-band notch antenna for automotive communications," *AEU-International Journal of Electronics and Communications*, vol. 80, pp. 104–113, 2017.
[37] G. P. Gao, M. K. Yang, S. F. Niu, and J. S. Zhang, "Study of a novel U-shaped monopole UWB antenna by transfer function and time domain characteristics," *Microwave and Optical Technology Letters*, vol. 54, no. 6, pp. 1532–1537, 2012.
[38] S. Kundu, "Experimental study of a printed ultra-wideband modified circular monopole antenna," *Microwave and Optical Technology Letters*, vol. 61, no. 5, pp. 1388–1393, 2019.
[39] R. R. Krishna and R. Kumar, "A slotted UWB monopole antenna with single port and double ports for dual polarization," *Engineering Science and Technology, an International Journal*, vol. 19, no. 1, pp. 470–484, 2016.
[40] M. S. Jameel, Y. S. Mezaal, and D. C. Atilla, "Miniaturized coplanar waveguide-fed UWB antenna for wireless applications," *Symmetry*, vol. 15, no. 3, p. 633, 2023.
[41] W. Balani, M. Sarvagya, A. Samasgikar, T. Ali, and P. Kumar, "Design and analysis of super wideband antenna for microwave applications," *Sensors*, vol. 21, no. 2, p. 477, 2021.
[42] A. Nella and A. S. Gandhi, "A five-port integrated UWB and narrowband antennas system design for CR applications," *IEEE Transactions on Antennas and Propagation*, vol. 66, no. 4, pp. 1669–1676, 2018.
[43] Z. N. Chen, N. Yang, Y. Guo, and M. Chia, "An investigation into measurement of handset antennas," *IEEE Transactions on Instrumentation and Measurement*, vol. 54, no. 3, pp. 1100–1110, 2005.

[44] S. Sharma and C. C. Tripathi, "An integrated frequency reconfigurable antenna for cognitive radio application," *Radioengineering*, vol. 26, no. 3, pp. 746–754, 2017.

[45] A. A. Abdulhameed, F. M. Alnahwi, H. L. Swadi, and A. S. Abdullah, "A compact cognitive radio UWB/reconfigurable antenna system with controllable communicating antenna bandwidth," *Australian Journal of Electrical and Electronics Engineering*, vol. 16, no. 1, pp. 1–11, 2019.

[46] Y. Jin and J. Choi, "A compact four-port coplanar antenna based on an excitation switching reconfigurable mechanism for cognitive radio applications," *Applied Sciences*, vol. 9, no. 15, p. 3157, 2019.

[47] R. K. Parida, R. K. Mishra, N. K. Sahoo, A. Muduli, D. C. Panda, and R. K. Mishra, "A hybrid multi-port antenna system for cognitive radio," *Progress in Electromagnetics Research C*, vol. 106, pp. 1–16, 2020.

[48] M. Abioghli, A. Keshtkar, M. Naser-Moghadasi, and B. Ghalamkari, "UWB rectangular DRA integrated with reconfigurable narrowband antenna for cognitive radio applications," *IETE Journal of Research*, vol. 67, no. 1, pp. 139–147, 2021.

[49] S. Lakrit, A. Nella, S. Das, B. T. P. Madhav, and C. Murali Krishna, "An integrated three-antenna structure for 5G, WLAN, LTE and ITU band cognitive radio communication," *AEU-International Journal of Electronics and Communications*, vol. 139, Article ID 153906, 2021.

[50] R. K. Parida, A. K. Sahu, D. K. Naik, P. Raiguru, D. C. Panda, and R. K. Mishra, "Compact reconfigurable antenna system for spectrum interweaved cognitive radio," *International Journal of RF and Microwave Computer-Aided Engineering*, vol. 32, no. 7, Article ID e23183, 2022.

[51] A. D. Tadesse, O. P. Acharya, and S. Sahu, "A five-port integrated planar ultra-wideband and narrowband antennas system using excitation switching reconfigurable technique for cognitive radio applications," *Wireless Personal Communications*, vol. 131, pp. 527–544, 2023.